Journal of Molecular Modeling (2020) 26: 254
https://doi.org/10.1007/s00894-020-04485-3

ORIGINAL PAPER

Spectral analysis and detailed quantum mechanical investigation of some acetanilide analogues and their self-assemblies with graphene and fullerene

Aljawhara H. Almuqrin[1] · Jamelah S. Al-Otaibi[2] · Y. Sheena Mary[3] · Renjith Thomas[4] · Savaş Kaya[5] · Dilara Özbakır Işın[6]

Received: 7 May 2020 / Accepted: 21 July 2020 / Published online: 2 September 2020

Abstract
Spectroscopic analysis and different quantum mechanical studies of four pharmaceutically active compounds phenacetin, p-acetanisidide, 4′-butoxyacetanilide, and 4′-(3-chloropropoxy)acetanilide are reported in this manuscript. Simulated IR spectrum of these compounds was compared with experimentally available data, and essential functional group assignments were made. We also report the frontier orbital properties and other derived local energy descriptors which talks about the relative stability and reactivity. Photovoltaic efficiency of the compounds was studied from the simulated electronic spectra. The compound was found to interact with graphene and fullerene, to form molecular self-assembly. These self-assemblies showed tremendous enhancement in various physicochemical properties when compared with its constituents. The nature of the interactions between studied chemical species was discussed with the help of chemical reactivity principles. Biological activity of the compounds was predicted using molecular docking studies. It is interesting to see that on adsorption with a graphene/fullerene surface, all adsorbed complex shows enhancement in the Raman activity giving surface enhanced Raman spectra (SERS). This can be used for the detection of these drugs in a pharmacological or biological sample. Interestingly the graphene/fullerene drug molecular assembly shows enhanced biological activity when compared with individual drug molecules.

Keywords DFT · Graphene · Fullerene · Acetanilide · Molecular docking

Introduction

Benzamide derivatives have biological and pharmacological activities such as inhibition of acetylcholinesterase, [1] antimicrobial, antioxidant [2], inhibition of chymotrypsin [3], antiasthmatic [4], and anti-human immunodeficiency virus activity [5]. A number of benzamide derivatives change the biological activity by changing substituents at the N-aryl and N-acyl part of benzamide moieties [6]. The benzamide derivatives, acetaminophen (paracetamol), and phenacetin are used as pain relievers and antipyretic drugs for the treatment of simple diseases and local issues like headaches, muscle pain, toothache, arthritis, and fever [7–9]. Long-period use of phenacetin can produce renal papillary necrosis, bladder tumors in humans, and some toxic effects [10–12]. Therefore, drugs containing phenacetin were withdrawn from the pharmacy in 1983 at the order of the US Food and Drug Administration (US FDA) [13]. Also, acetaminophen (N-acetyl-p-aminophenol) is the most widely used prescription pain medicine in the USA. Such pharmaceutically active anthropogenic compounds are

Electronic supplementary material The online version of this article (https://doi.org/10.1007/s00894-020-04485-3) contains supplementary material, which is available to authorized users.

✉ Y. Sheena Mary
marysheena2018@rediffmail.com

1 Department of Physics, College of Science, Princess Nourah bint Abdulrahman University, Riyadh, Saudi Arabia

2 Department of Chemistry, College of Science, Princess Nourah bint Abdulrahman University, Riyadh, Saudi Arabia

3 Department of Physics, Fatima Mata National College (Autonomous), Kollam, Kerala, India

4 Department of Chemistry, St. Berchmans College (Autonomous), Changanacherry, Kerala, India

5 Department of Pharmacy, Sivas Cumhuriyet University, Health Services Vocational School, 58140 Sivas, Turkey

6 Department of Chemistry, Sivas Cumhuriyet University Faculty of Science, Sivas, Turkey

commonly detected in different environmental segments such as surface water, groundwater, and soil [14].

Graphene is basically a monoatomic graphite layer, a carbon allotrope of carbon atoms tightly attached in hexagonal lattice. Sp^2 hybridization and atomic thickness graphene of 0.3 nm make it a quite different kind material [15]. Providing larger surface area for adsorbing pharmaceutical contaminant materials makes graphene as desirable substrate for use in water treatment. In literature, extensive research has been reported on graphene membranes for water treatment [16–18]. Due to its graphical hydrophobic surface and strong π-π interaction, it shows high adsorption property to chemicals. Here, density functional theory (DFT) calculations were used to examine interactions of selected acetanilide derivatives, phenacetin (PHE), p-acetanisidide (AAS), 4′-butoxyacetanilide (BAN), and 4′-(3-chloropropoxy)acetanilide (CPA) on surface of atomic thickness graphene/fullerene. The current work provides a comprehensive analysis on interaction of adsorbed acetanilide derivatives with graphene/fullerene. Systems like fullerenes, nanotubes, and graphene are of immense applications in the chemical industry due to their practical utilities [19–21]. Fullerene nanostructures have been especially prevalent in scientific literature and have thus far demonstrated the capacity to be applied to solve some of the emerging challenges facing humanity. These systems are found to adsorb even a large variety of pollutants with high binding energies [22–26]. Enhancement of Raman spectra was also absorbed in the case of these molecules, when they get adsorbed on the surface of the graphene sheet [27]. This manuscript deals with a detailed structure and geometry analysis of these compounds. Different spectral observations like UV, IR, and Raman were also theoretically examined using various computational tools.

Methods of calculation

The geometry of the molecules, PHE, AAS, BAN, CPA, and their self-assemblies are optimized from an initial guess structure using various using DFT with B3LYP functional [28, 29], and 6–311++G(d,p) basis sets using Gaussian09 software [30] and GaussView [31] as the user interface. The optimized structure of PHE, AAS, BAN, and CPA is given in Fig. 1. The electronic spectra were simulated with CAM-B3LYP with the same basis set from the optimized geometry in solvent methanol using the Integral Equation Formalism Polarizable Continuum Model (IEFPCM) [32] in TD-DFT formalism. The spectral data of PHE, AAS, BAN, and CPA are derived from Spectrabase [33]. ω-B97XD, which incorporates dispersion correction, was selected to analyze self-assembly of molecules with graphene and fullerene [34].

Energy descriptors and NLO properties

Highest occupied molecular orbital (HOMO)-lowest unoccupied molecular orbital (LUMO) gives molecular chemical stability and gives bioactivity and charge transfer. A molecule that has a small energy gap has high chemical reactivity [35, 36]. The HOMO-LUMO diagram is displayed in Fig. S1. For all the molecules, HOMO is delocalized over the ring portions and attached groups and while the LUMO is only over the ring portions and the nature changes from HOMO to LUMO transitions. HOMO and LUMO energies are − 7.972 and − 4.545 eV for PHE, − 7.958 and − 4.545 eV for AAS, − 7.973 and − 4.545 eV for BAN, and − 7.976 and − 4.547 eV for CPA. The band gap energy is around 3.420 eV for all derivatives. The various quantum chemical parameters

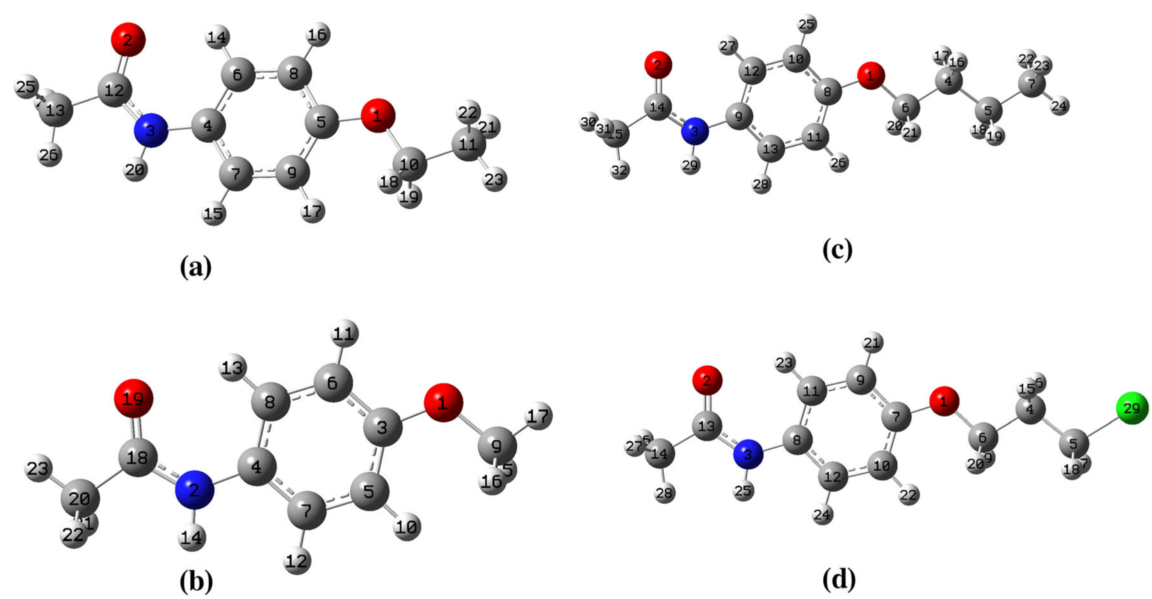

Fig. 1 Optimized structure of **a** PHE, **b** AAS, **c** BAN, and **d** CPA

Table 1 Chemical descriptors

Molecule	I = − EHOMO	A = − ELUMO	Energy gap	η = (I − A)/2	μ = − (I + A)/2	ω = μ²/2η
PHE	7.972	4.545	3.427	1.713	− 6.259	11.430
AAS	7.958	4.545	3.412	1.706	− 6.252	11.453
BAN	7.973	4.545	3.428	1.714	− 6.259	11.429
CPA	7.976	4.547	3.429	1.714	− 6.262	11.434
PHE-G	7.979	5.727	1.252	1.126	− 6.853	20.852
AAS-G	7.979	5.728	2.251	1.125	− 6.853	20.869
BAN-G	7.987	5.725	2.262	1.131	− 6.856	20.783
CPA-G	7.978	5.728	2.249	1.125	− 6.853	20.879
PHE-F	7.628	6.918	0.709	0.355	− 7.273	74.564
AAS-F	7.618	6.914	0.704	0.352	− 7.266	75.006
BAN-F	7.621	6.916	0.706	0.353	− 7.269	74.877
CPA-F	7.629	6.914	0.715	0.357	− 7.272	74.000

obtained using energy gap are shown in Table 1. The low bandgap suggests that these compounds have more bioactive and used for disinfectant in water treatment [36]. The electrophilicity index value around 11.400 eV suggests the biological activity of the compounds.

Most of the organic compounds possess nonlinear optical (NLO) properties and polarizability and hyperpolarizability are given in Table 2 [37, 38]. First-order hyperpolarizability ($\times 10^{-30}$ esu) changes in the order: BAN (10.159) > PHE (9.044) > CPA (8.565) > AAS (6.893) which are 78, 70, 66, and 53 times that of urea, while the second-order values are -8.626×10^{-37}, -6.318×10^{-37}, -15.247×10^{-37}, and -19.498×10^{-37} for PHE, AAS, BAN, and CPA [39].

We used the time-dependent DFT method to simulate the ultraviolet-visible and density of states (DOS) spectra (Fig. S2 and Fig. S3) of the PHE, AAS, BAN, and CPA using CAM-B3LYP/6–311++G(d,p) basis set using an implicit solvation model with methanol solvent atmosphere. Density of state diagrams shows that there is clear distinction between the HOMO and LUMO. Also, no overlap between the core orbitals was observed. For these compounds, PHE, AAS, BAN, and CPA, there are three electronic excitations, but the one around 234 nm is with the maximum oscillator strengths (f) of 0.6346, 0.5742, 0.6635, and 0.6699 which belongs to the HOMO to LUMO transition (89, 82, 89, and 88%). In these compounds, the HOMO is located at the pi bonding orbitals of the phenyl ring and in the side chains, and LUMO is at the pi antibonding orbitals present in the phenyl rings. This is an excellent pi to pi antibonding transition, which may lead to intra-molecular

Table 2 NLO properties

Molecule	Dipole moment	Polarizability first order		Second order
–	(Debye)	–	Hyperpolarizability	Hyperpolarizability
–	–	($\times 10^{-23}$ esu)	($\times 10^{-30}$ esu)	($\times 10^{-37}$ esu)
PHE	5.3628	2.047	9.044	− 8.626
AAS	5.5001	1.839	6.893	− 6.318
BAN	5.3701	2.415	10.159	− 15.247
CPA	6.4954	2.413	8.565	− 19.498
PHE-G	5.9014	6.378	7.917	− 40.732
AAS-G	6.4468	5.414	5.789	− 37.891
BAN-G	5.5773	6.695	8.522	− 46.465
CPA-G	6.1955	5.843	7.105	− 53.819
PHE-F	5.8397	4.501	29.647	− 43.766
AAS-F	6.3093	4.393	57.989	− 38.043
BAN-F	6.5156	4.899	47.432	− 56.108
CPA-F	4.5069	4.762	11.826	− 53.712

charge transfer. Data from electronic spectra (Table S1) can be used to model the photovoltaic efficiency of a compound. For the title compounds, the f value, around 233 nm, is in the range 0.5742–0.6639, and the LHE is in the range 0.7334–0.7862. The free energy of electron injection, ΔG_{inject} in kcal/mol, is − 53.7999, − 54.4917, − 54.0005, and − 52.9444 for PHE, AAS, BAN and CPA, respectively, which shows good photosensitizing property [40–43].

IR and Raman spectra

The detailed assignment of vibrations obtained from the scaled simulated spectrum and experimental spectrum is provided in Table S2. The vibrations at 3290 cm^{-1} (IR), 3390 cm^{-1} (Raman), and 3480 cm^{-1} (DFT) for PHE; 3280 cm^{-1} (IR) and 3468 cm^{-1} (DFT) for AAS; 3300 cm^{-1} (IR) and 3480 cm^{-1} (DFT) for BAN; and 3290 cm^{-1} (IR) and 3480 cm^{-1} (DFT) cm^{-1} for CPA are the NH stretches [44]. For all the molecules, NH deformation mode is in the range 1511–1507 cm^{-1} theoretically and observed around 1510 cm^{-1} [44]. The υC=O is at 1620 cm^{-1} (Raman) and 1611 cm^{-1} (DFT) for PHE, 1608 cm^{-1} (IR) and 1617 cm^{-1} (DFT) for AAS, 1565 cm^{-1} (IR) and 1574 cm^{-1} (DFT) for BAN, and 1570 cm^{-1} (IR) and 1575 cm^{-1} (DFT) for CPA [44]. The C–O stretches are assigned at 1177 and 1013 cm^{-1} for PHE, 1152 and 975 cm^{-1} for AAS, 1177and 960 cm^{-1} for BAN, and 1205 and 977 cm^{-1} for CPA theoretically, while bands are seen at 1185 and 1020 cm^{-1} for PHE, 1154 and 973 cm^{-1} for AAS, 1175 and 965 cm^{-1} for BAN, and 1205 and 970 cm^{-1} for CPA experimentally [44].

Adsorption behavior of molecules on the surface of graphene/fullerene

Graphene is a 2D layer of graphite which contains carbon atoms in sp2 hybridized fashion. It is found experimentally that many molecules get adsorbed over the graphene sheet and form self-assembly. This unique property can be used for the detection of these compounds in a condensed phase or its removal [45–51]. Fullerene also shows the formation of a self-assembly. The energetics of the adsorption of the two compounds are discussed as follows. The adsorption energy is given in Table S3 [52]. The adsorption energy is maximum for PHE-G and BAN-G complexes, and the least is for other G and F complexes. It is evident from the simulated electronic spectra that, compounds with graphene complex, the oscillator strengths (Table S4) of AAS-G and CPA-G are greater than one, for the electronic transitions at 273.88 and 269.30 nm, and the LHE were found to be above 92%, while for PHE-G and BAN-G complexes, LHE is less than 75%. The ΔG_{inject} is high for PHE-G and BAN-G, and these derivatives can be effectively used as a higher photosensitizer with respect to the pristine molecules.

For graphene-molecule assembly, HOMO is located over the drug molecules, and LUMO is over the graphene layer, while for fullerene-molecule assembly, HOMO and LUMO are over the fullerene with interchanging the positions. Chemical potential (Table 1) value is more negative for fullerene complex with PHE, AAS, BAN, and CPA, which means more stability. Also, the electrophilicity indices of graphene/fullerene self-assembly with PHE, AAS, BAN, and CPA are increasing with respect to the pristine values. For fullerene complexes, there is very high enhancement for this index. Also, the hardness values decrease for graphene/fullerene complexes.

Surface enhanced Raman scattering (SERS) data (Table S5) demonstrates improved Raman signals for multiple wavenumbers in both graphene and fullerene complexes. Figures S4, S5, S6, and S7 give the Raman spectra (normal and enhanced), UV, DOS, and HOMO-LUMO of the graphene/fullerene assembly. For A8-graphene complex, intensity multiplication is for 1319 cm^{-1} from 2.73 to 51.41, with and enhancement factor of 1783, which is significant, while this mode is not seen in PHE-fullerene complex. Multiplication of 1061 is seen for 3053 cm^{-1} in PHE-G complex, which corresponds to υCH with blue shift of wavenumber to 3073 cm^{-1}, and for PHE-fullerene complex, this mode is enhanced with an enhancement factor of 122. For AAS-G, the in-pane CH deformation at 1314 cm^{-1} undergoes a shift to 1332 cm^{-1} with an enhancement factor of 2425, while 1321 cm^{-1} of AAS-F undergoes a shift to 1325 cm^{-1} with a lower enhancement factor of 160. In AAS-G, C=O stretch has an enhancement of 510, while in fullerene complex, the enhancement for this mode is only 360. In BAN-G complex, the ring stretching and CH stretch at 1319 cm^{-1} and 3052 cm^{-1} undergo wavenumber shift with enhancement factors 1488 and 1471. In the corresponding fullerene complex, no such large enhancement is observed, but the CH3 bending mode at 1451 cm^{-1} has an enhancement factor of 1423. In CPA-G, CH2 bending mode has an enhancement of 1602, and in fullerene, the corresponding enhancement for CH2 modes are 742 and 308. This indicates that it is possible to make a graphene or fullerene-based sensor for the detection of these compounds using SERS [53].

Molecular docking

Prediction of activity spectra (PASS) analysis [54] gives activities, CYP2C12 substrate, membrane integrity agonist, and CYP2F1 substrate (activity values 0.927, 0.914 and 0.907). 5VBU, 2Y02, and 2PG5 were used for docking by PatchDock Server [55, 56] of the molecules using the selected PDB's [57, 58]. The ligand-substrates interactions are given in Table S6. The global energy and atomic contact energy of the graphene/fullerene complexes are higher than that of parent molecules. The docked ligands with the receptors and at the active site are shown in Fig. S8 and Fig. S9. The global energy value of ligand (parent molecules) with CYP2C12 substrate, membrane integrity agonist, and CYP2F1 substrate are − 40.22, − 36.50, and − 22.38 kcal/mol for PHE; − 37.53, − 32.66, and − 21.39 kcal/mol for AAS; − 37.32, − 39.38, and − 27.00 kcal/mol for BAN; and − 40.69, − 31.66, and − 28.59 kcal/mol for CPA (Table 3). Such findings indicate that the compounds have inhibitory effect against the receptors.

Table 3 Energy values given by PatchDock

Compound –	PDB –	Global energy	aVdW –	rVdW –	Atomic contact energy
PHE	5VBU	− 40.22	− 14.60	0.31	− 11.90
	2Y02	− 36.50	− 13.20	1.62	− 12.63
	2PG5	− 22.38	− 10.35	5.08	− 7.42
AAS	5VBU	− 37.52	− 14.61	4.59	− 12.37
	2Y02	− 32.66	− 11.69	0.96	− 10.90
	2PG5	− 21.39	− 10.26	4.25	− 6.20
BAN	5VBU	− 37.32	13.86	1.26	− 11.24
	2Y02	− 39.38	− 13.76	0.96	− 13.99
	2PG5	− 27.00	− 11.03	3.66	− 8.71
CPA	5VBU	− 40.69	− 16.25	4.28	− 12.40
	2Y02	− 31.66	− 12.61	2.57	− 11.29
	2PG5	− 28.59	− 11.53	2.65	− 8.95
PHE-G	5VBU	− 72.30	− 25.23	3.89	− 23.52
	2Y02	− 56.37	− 27.15	2.49	− 12.00
	2PG5	− 74.61	− 25.70	4.07	− 24.69
AAS-G	5VBU	− 69.80	− 25.85	9.44	− 24.20
	2Y02	− 58.56	− 29.90	5.89	− 11.70
	2PG5	− 76.71	− 27.16	3.89	− 24.57
BAN-G	5VBU	− 74.77	− 27.05	8.23	− 25.51
	2Y02	− 78.72	− 26.72	3.63	− 26.11
	2PG5	− 78.72	− 26.72	3.63	− 26.11
CPA-G	5VBU	− 68.76	− 28.56	13.22	− 23.29
	2Y02	− 60.95	− 22.73	4.97	− 20.29
	2PG5	− 80.90	− 28.91	5.64	− 26.31
PHE-F	5VBU	− 69.95	− 26.41	7.75	− 22.84
	2Y02	− 61.20	− 23.23	10.87	− 22.53
	2PG5	− 79.63	− 29.46	8.12	− 26.25
AAS-F	5VBU	− 71.02	− 26.01	5.94	− 23.06
	2Y02	− 55.29	− 19.95	7.29	− 20.45
	2PG5	− 75.85	− 27.26	4.38	− 24.06
BAN-F	5VBU	− 75.05	− 30.88	5.59	− 21.09
	2Y02	− 55.79	− 26.84	4.21	− 12.28
	2PG5	− 80.99	− 30.84	10.80	− 27.17
CPA-F	5VBU	− 74.55	− 27.27	5.46	− 23.90
	2Y02	− 54.89	− 28.84	13.29	− 15.03
	2PG5	*− 85.03*	*− 31.56*	*7.22*	*− 27.21*

[a] VdW and rVdW—softened attractive and repulsive van der Waals energy

Conclusion

We report all studies using the optimized geometry of the most stable conformer. The experimental and scaled simulated IR spectrum showed close agreement. Among the four compounds, 4′-butoxyacetanilide shows highest light-harvesting efficiency, but the free energy of electron injection is more for p-acetanisidide. When compared with parent compounds, self-assemblies of the compounds with graphene and fullerene showed significant enhancement in all physical, chemical, and biological activities. There was an enhancement in the Raman intensity of the compounds, which enables the way for designing various detection methods using SERS. The calculations made showed that the studied molecules interact more powerful with graphene compared with fullerene. Docking studies reveal the inhibitory effect against receptors.

Funding The authors would like to thank the Center for Promising Research in Social Research and Women's Studies Deanship of Scientific Research, at Nourah bint Abdulrahman University, for funding this project in 2020.

Compliance with ethical standards

Conflict of interest The authors declare that they have no conflict of interest.

References

1. Gao XH, Liu LB, Liu HR, Tang JJ, Kang L, Wu H, Cui P, Yan J (2018) Structure-activity relationship investigation of benzamide and picolinamide derivatives containing dimethylamine side chain asacetylcholinesterase inhibitors. J. Enzyme Inhib. Med. Chem. 33: 110–114
2. Yang X, Peng T, Yang Y, Li W, Xiong J, Zhao L, Ding Z (2015) Antimicrobial and antioxidant activities of a new benzamide from endophytic Streptomyces sp. YIM 67086. Nat. Prod. Res. 29:331–335
3. Lum RT, Nelson MG, Joly A, Horsma AG, Lee G, Meyer SM, Wick MM, Schow SR (1998) Selective inhibition of the chymotrypsin-like activity of the 20S proteasome by 5-methoxy-1-indanone dipeptide benzamides. Bioorg. Med. Chem. Lett. 8: 209–214
4. Ashton MJ, Cook DC, Fenton G, Karisson JA, Palfreyman MN, Raeburn D, Ratcliffe AJ, Soness JE, Thurairatnam S, Vicker N (1994) Selective type IV phosphodiesterase inhibitors as antiasthmatic agents. The syntheses and biological activities of 3-(cyclopentyloxy)-4-methoxybenzamides and analogs. J. Med. Chem. 37:1696–1703
5. Tummino PJ, Harvey PJ, McQuade T, Domagala J, Gogliotti R, Sanchez J, Song Y, Hupe D (1997) The human immunodeficiency virus type1 (HIV-1) nucleocapsid protein zinc ejection activity of disulfide benzamides and benzisothiazolones: correlation with anti-HIV and virucidal activities. Antimicrob. Agents Chemother. 41: 394–400
6. Wajid S, Khatoon A, Khan MA, Zafar H, Kanwal S, Choudhary MI, Basha FZ (2019) Microwave-assisted organic synthesis, structure–activity relationship, kinetics and molecular docking

studies of non-cytotoxic benzamide derivatives as selective butyrylcholinesterase inhibitors. Bioorg. Med. Chem. 27:4030–4040
7. Seegers AJ, Jager LP, Zandberg P, van Noordwijk J (1981) The anti-inflammatory, analgesic and antipyretic activities of non-narcotic analgesic drug mixtures in rats. Arch. Int. Pharmacodyn. Ther. 251:237–254
8. Velázquez F, Manríquez R, Maya L, Barrientos L, López-Dellamary F (2009) Phenacetin isolated from Bursera grandifolia, a herbal remedy with antipyretic properties. Nat. Prod. Commun. 4: 1575–1576
9. Clissold SP (1986) Paracetamol and phenacetin. Drugs 32:46–59
10. Dolora P, Lodovici M, Salvadori M, Saltutti C, Rose AD, Selli C, Kriebel D (1998) Variations of cartisol hydroxylation and paracetamol metabolism in patients with bladder carcinoma. Br. J. Urol. 62:419–426
11. Grimland K (1998) Phenacetin and renal damage at a Swedish factory. Acta Med. Scand. 174:1–26
12. Sicardi SM, Martiarena JL, Iglesias MT (1991) Mutagenic and analgesic activities of aniline derivatives. J. Pharm. Sci. 80:761–764
13. FDA (1999) List of drug products that have been withdrawn or removed from the market for reasons of safety or effectiveness. Fed. Regist. 64:10944–10947 https://www.ncbi.nlm.nih.gov/pubmed/10557618
14. Kaufman DW, Kelly JP, Rosenberg L, Anderson TE, Mitchell AA (2002) Recent patterns of medication use in the ambulatory adult population of the United States: the Slone survey. JAMA 287:337–344
15. Zhu H, Xu Z, Xie D, Fang Y (2018) Graphene: fabrication, characterizations, properties and applications. Academic Press, London
16. Nicolai A, Sumpter BG, Meunier V (2014) Tunable water desalination across graphene oxide framework membranes. Phys. Chem. Chem. Phys. 16:8646–8654
17. Martin MJ, May S, Mebberson N, Pendleton P, Vasileve K, Plush SE, Hayball JD (2017) Activated carbon, carbon nanotubes and graphene: materials and composites for advanced water purification. J. Carbon Res. 3:1–29
18. Reddy AVB, Moniruzzaman M, Reddy YVM, Madhavi G (2019) Graphene-based nanomaterials for the removal of pharmaceuticals in drinking water sources, in graphene-based nanotechnologies for energy and environmental applictions, pp. 329-358, Elsevier
19. Al-Jumaili A, Alancherry S, Bazaka K, Jacob M (2017) Review on the antimicrobial properties of carbon nanostructures. Materials 10: 1066
20. Ahamadi R, Sarvestani MRJ, Sadeghi B (2018) Computational study of the fullerene effects on the properties of 16 different drugs: a review. Int. J. Nano Dimens. 9:325–335
21. Sun Q, Zhang R, Qiu J, Liu R, Xu W (2018) On-surface synthesis of carbon nanostructures. Adv. Mater. 30:1705630
22. El-Mahdy A (2016) Density functional investigation of CO and NO adsorption on TM-decorated C60 fullerene. Appl. Surf. Sci. 383: 353–366
23. Lin IH, Lu YH, Chen HT (2017) Nitrogen doped C60 as a robust catalyst for CO oxidation. J. Comput. Chem. 38:2041–2046
24. Hwang DG, Jeong E, Lee SG (2016) Density functional theory study of CH4 and CO2 adsorption by fluorinated graphene. Carbon Lett. 20:81–85
25. Zahedi E, Seif A (2011) Adsorption of NH3 and NO2 molecules on C48B6N6 heterofullerene: a DFT study on electronic properties. Phys. B 406:3704–3709
26. Ramachandran C, Sathyamurthy N (2007) Time dependent density functional theoretical study of the absorption properties of BN substituted C60 fullerenes. J. Phys. Chem. A 111:6901–6903
27. Jiang Y, Wang J, Malfatti L, Carboni D, Senes N, Innocenzi P (2018) Highly durable graphene-mediated surface enhanced Raman scattering (G-SERS) nano composites for molecular detection. Appl. Surf. Sci. 450:451–460
28. Becke AD (1993) Density functional thermo chemistry. III. The role of exact exchange. J. Chem. Phys. 98:5648–5652
29. Lee C, Yang W, Parr RG (1988) Development of the Colle-Salvetti correlation energy formula into a functional of the electron density. Phys. Rev. B37:785–789
30. Frisch MJ, Trucks GW, Schlegel HB, Scuseria GE, Robb MA, Cheeseman JR, Scalmani G, Barone V, Mennucci B, Petersson GA, Nakatsuji H, Caricato M, Li X, Hratchian HP, Izmaylov AF, Bloino J, Zheng G, Sonnenberg JL, Hada M, Ehara M, Toyota K, Fukuda R, Hasegawa J, Ishida M, Nakajima T, Honda Y, Kitao O, Nakai H, Vreven T, Montgomery Jr JA, Peralta JE, Ogliaro F, Bearpark M, Heyd JJ, Brothers E, Kudin KN, Staroverov VN, Keith T, Kobayashi R, Normand J, Raghavachari K, Rendell A, Burant JC, Iyengar SS, Tomasi J, Cossi M, Rega N, Millam JM, Klene M, Knox JE, Cross JB, Bakken V, Adamo C, Jaramillo J, Gomperts R, Stratmann RE, Yazyev O, Austin AJ, Cammi R, Pomelli C, Ochterski JW, Martin RL, Morokuma K, Zakrzewski VG, Voth GA, Salvador P, Dannenberg JJ, Dapprich S, Daniels AD, Farkas O, Foresman JB, Ortiz JV, Cioslowski J, Fox DJ (2010) Gaussian 09, revision B.01. Gaussian, Inc, Wallingford
31. Keith T, Millam J (2009) Gaussview 5, Semichem. Inc. Shawnee Mission KS
32. Al-Otaibi JS, Mary YS, Mary YS, Thomas R (2019) Quantum mechanical and photovoltaic studies on the cocrystals of hydrochlorothiazide with isonazid and malonamide. J. Mol. Struct. 1197: 719–726
33. Bio-Rad Laboratories, Inc., SpectraBase; http://spectrabase.com/. Acessed 15 July 2019
34. Chai JD, Head-Gordon M (2008) Long-range corrected hybrid density functionals with damped atom-atom dispersion corrections. Phys. Chem. Chem. Phys. 10:6615–6620
35. Thomas R, Hossain M, Mary YS, Resmi KS, Armakovic S, Armakovic SJ, Nanda AK, Ranjan VK, Vijayakumar G, Van Alsenoy C (2018) Spectroscopic analysis and molecular docking of imidazole derivatives and investigation of its reactive properties by DFT and molecular dynamics simulations. J. Mol. Struct. 1158: 156–175
36. Shafieyoon P, Mehdipour E, Mary YS (2019) Synthesis, characterization and biological investigation of glycine based sulfonamide derivative and its complex: vibration assignment, HOMO-LUMO analysis, MEP and molecular docking. J. Mol. Struct. 1181:244–252
37. Zhang T, Wei X, Zuo Y, Chao J (2019) An efficient measure to improve the NLO performance by point charge electric field. Optik 182:295–302
38. Mary YS, Mary YS, Thomas R, Narayana B, Samshuddin S, Sarojini BK, Aramkovic S, Armakovic SJ, Pillai GG (2019) Theoretical studies on the structure and various physic-chemical and biological properties of a terphenyl derivative with immense anti-protozoan activity. Polycycl. Aromat. Compd. https://doi.org/10.1080/10406638.2019.1624974
39. Hossain M, Thomas R, Mary YS, Resmi KS, Aramkovic S, Armakovic SJ, Nanda AK, Vijayakumar G, Van Alsenoy C (2018) Understanding reactivity of two newly synthetized imidazole derivatives by spectroscopic characterization and computational study. J. Mol. Struct. 1158:176–196
40. Louazri L, Amine A, Bouzzine SM, Hamidi M, Bouachrine M (2016) Photovoltaic properties of Zn-complexed-phtalocyanine and derivatives for DSSCs application. J. Mater. Environ. Sci. 7: 2305–2313
41. Ren XF, Zhang J, Kang GJ (2015) Theoretical studies of electronic structure and photophysical properties of a series of indoline dyes with triphenylamine ligand. J. Nanomater.:605727. https://doi.org/10.1155/2015/605728

42. Chaitanya K, Ju XH, Heron BM (2015) Can elongation of the π-system in triarylamine derivated sensitizers with either benzothiadiazole and/or ortho-fluorophenyl moieties enrich their light harvesting efficiency? – a theoretical study. RSC Adv. 5: 3978–3998
43. Mary YS, Ertan-Bolelli T, Thomas R, Krishnan AR, Bolelli K, Kasap EN, Onkol T, Yildiz I (2019) Quantum mechanical studies of three aromatic halogen-substituted bioactive sulfonamidobenzoxazole compounds with potential light harvesting properties. Polycycl. Aromat. Compd. https://doi.org/10.1080/10406638.2019.1689405
44. Roeges NPG (1994) A guide to the complete interpretation of infrared spectra of organic structures. Wiley, New York
45. Fleischmann M, Hendra PJ, McQuillan AJ (1974) Raman spectra of pyridine adsorbed at a silver electrode. Chem. Phys. Lett. 26: 163–166
46. Albrecht MG, Creighton JA (1977) Anomalously intense Raman spectra of pyridine at a silver electrode. J. Am. Chem. Soc. 99: 5215–5217
47. Jeanmaire DL, Van Duyne RP (2006) Surface Raman spectro electrochemistry. J. Electroanal. Chem. Interfacial Electrochem. 84:1–20
48. Smith E, Dent G (2005) Modern Raman spectroscopy – a practical approach. https://doi.org/10.1002/0470011831
49. Kneipp K, Wang Y, Kneipp H, Perelman LT, Itzkan I, Dasari RR, Feld MS (1997) Single molecule detection using surface enhanced Raman scattering (SERS). Phys. Rev. Lett. 78:1667–1670
50. Nie S, Emory SR (1997) Probing single molecules and single nano particles by surface enhanced Raman scattering. Science 275:1102–1106
51. Novoselov KS, Geim AK, Morozov SV, Jiang D, Zhang Y, Dubonos SV, Grigorieva IV, Firsov AA (2004) Electric field in atomically thin carbon films. Science 306:666–669
52. Sharma V, Som NN, Pillai SB, Jha PK (2020) Utilization of doped GQDs for ultrasensitive detection of catastrophic melamine: a new SERS platform. Spectrochim. Acta 224:117352
53. Al-Otaibi JS (2020) Detailed quantum mechanical studies on bioactive benzodiazepine derivatives and their adsorption over graphene sheets. Spectrochim. Acta 235:118333
54. Lagunin A, Stepanchikova A, Filimonov D, Poroikov V (2000) PASS: prediction of activity spectra for biologically active substances. Bioinformatics 16:747–748
55. Duhovny D, Nussinov R, Wolfson HJ (2000) Efficient unbound docking of rigid molecules, in: Gusfield et al. (Eds.), Proceedings of the second workshop on algorithms in bioinformatics (WABI) Rome, Italy, lecture notes in computer science, vo. 2452, Springer Verlag, pp.185-200
56. Schneidman-Duhovny D, Inbar Y, Nussinov R, Wolfson HJ (2005) Patchdock and Symmdock: servers for rigid and symmetric docking. Nucleic Acids Res. 33:W363–W367
57. Mary YS, Mary YS, Resmi KS, Kumar VS, Thomas R, Sureshkumar B (2019) Detailed quantum mechanical, molecular docking, QSAR prediction, photovoltaic light harvesting efficiency analysis of benzil and its halogenated analogues. Heliyon 5:e2825
58. Mary YS, Mary YS, Resmi KS, Thomas R (2019) DFT and molecular docking investigations of oxicam derivatives. Heliyon 5: e02175